The Geological Society of America
Special Paper 509
2015

Regional seismic-wave propagation from the M5.8 23 August 2011, Mineral, Virginia, earthquake

Fred F. Pollitz
Walter D. Mooney
U.S. Geological Survey, 345 Middlefield Road, MS 977, Menlo Park, California 94025, USA

ABSTRACT

The M5.8 23 August 2011 Mineral, Virginia, earthquake was felt over nearly the entire eastern United States and was recorded by a wide array of seismic broadband instruments. The earthquake occurred ~200 km southeast of the boundary between two distinct geologic belts, the Piedmont and Blue Ridge terranes to the southeast and the Valley and Ridge Province to the northwest. At a dominant period of 3 s, coherent postcritical P-wave (i.e., direct longitudinal waves trapped in the crustal waveguide) arrivals persist to a much greater distance for propagation paths toward the northwest quadrant than toward other directions; this is probably related to the relatively high crustal thickness beneath and west of the Appalachian Mountains. The seismic surface-wave arrivals comprise two distinct classes: those with weakly dispersed Rayleigh waves and those with strongly dispersed Rayleigh waves. We attribute the character of Rayleigh wave arrivals in the first class to wave propagation through a predominantly crystalline crust (Blue Ridge Mountains and Piedmont terranes) with a relatively thin veneer of sedimentary rock, whereas the temporal extent of the Rayleigh wave arrivals in the second class are well explained as the effect of the thick sedimentary cover of the Valley and Ridge Province and adjacent Appalachian Plateau province to its northwest. Broadband surface-wave ground velocity is amplified along both north-northwest and northeast azimuths from the Mineral, Virginia, source. The former may arise from lateral focusing effects arising from locally thick sedimentary cover in the Appalachian Basin, and the latter may result from directivity effects due to a northeast rupture propagation along the finite fault plane.

INTRODUCTION

The M5.8 23 August 2011 Mineral (Virginia, USA) earthquake is the largest event to have struck Virginia since 1897. The seismic waves generated by the event were felt as far away as New York and Montreal and were recorded by regional broadband instruments (Fig. 1). Observations of broadband seismic waveforms as much as 900 km from the epicenter complement observations of felt intensities (Hough, 2012) and provide a unique opportunity to characterize the regional seismic-wave propagation, test current models of the seismic structure, and better understand the factors that lead to variable seismic-wave amplitude and duration.

Pollitz, F.F., and Mooney, W.D., 2015, Regional seismic wave propagation from the M5.8 23 August 2011, Mineral, Virginia, earthquake, *in* Horton, J.W., Jr., Chapman, M.C., and Green, R.A., eds., The 2011 Mineral, Virginia, Earthquake, and Its Significance for Seismic Hazards in Eastern North America: Geological Society of America Special Paper 509, p. 95–116, doi:10.1130/2015.2509(06). For permission to copy, contact editing@geosociety.org. © 2014 The Geological Society of America. All rights reserved.

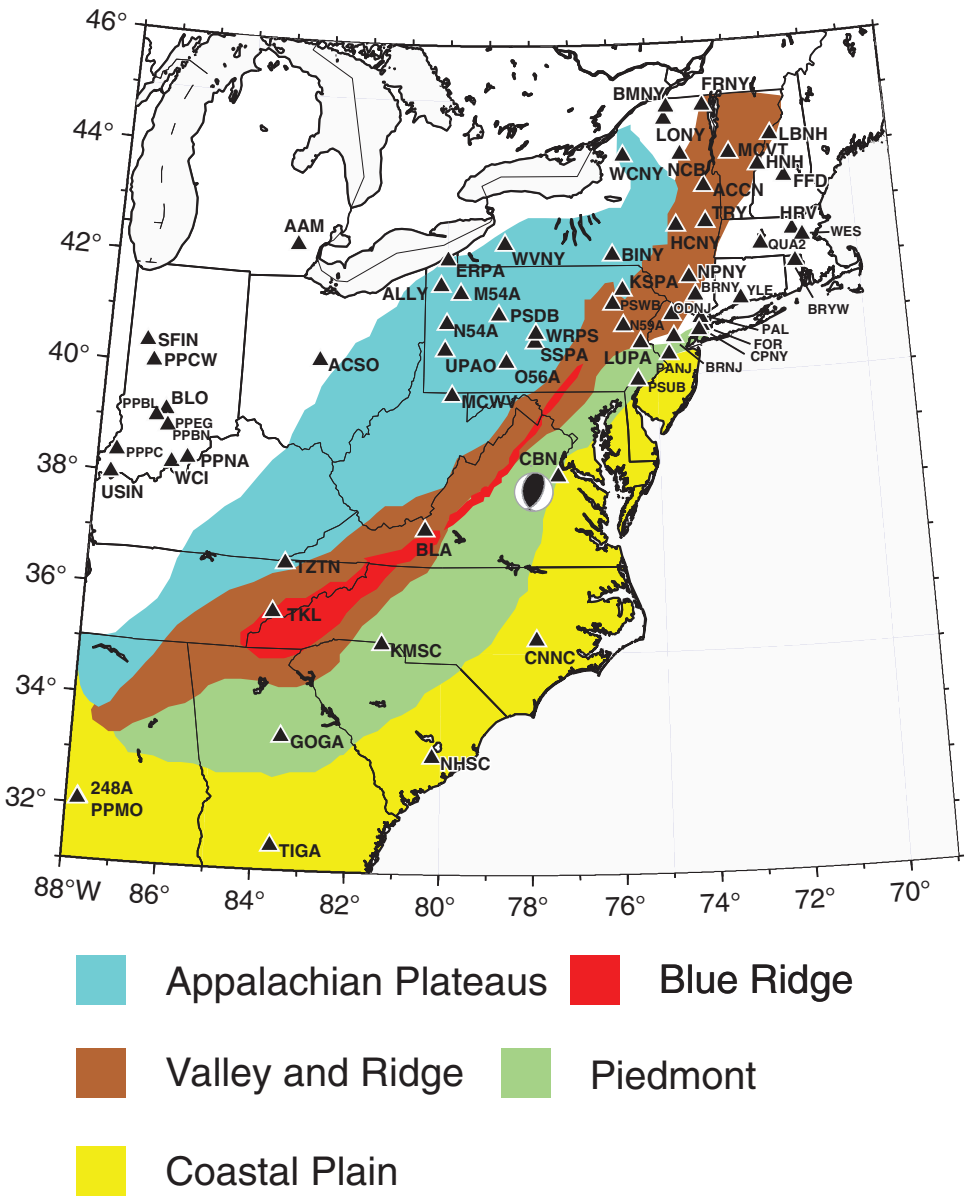

Figure 1. Seismic stations (triangles) with three-component seismograms analyzed in this study. The beachball symbol indicates the epicenter and focal mechanism of the 2011 Virginia earthquake taken from the USGS/SLU (U.S. Geological Survey/Saint Louis University) Regional Moment Solution. The regional physiographic provinces are superimposed.

The earthquake involved high-angle reverse slip on an ~10-km long, 45° east-southeast–dipping fault between 2.5 and 8 km depth. It occurred in the eastern Piedmont thrust sheet within a belt of Triassic basins. Thrust faulting in such a passive continental margin is often thought to represent reactivation of ancient structures associated with continental collision or rifting (e.g., Cloetingh et al., 2008; Bailey and Owens, 2012). Delineation of the fault plane through precise aftershock locations suggests that the causative fault dips more steeply than known thrust structures and therefore did not reactivate a Paleozoic thrust (Ellsworth et al., 2011). Rather, the rupture may have occurred at the contact between the Paleozoic Goochland (Glover et al., 1982; Farrar, 1984; Farrar and Owens, 2001) and Chopawamsic terranes (Pavlides, 1981; Coler et al., 2000), which are divided by the Spotsylvania zone, a steeply dipping high-strain zone (Neuschel, 1970).

The seismic structure in the epicentral area is defined by the igneous and metasedimentary rocks that make up the Piedmont and Blue Ridge terranes (Fig. 1), which are characterized by a modest sedimentary cover of <~1 km. Further west, this structure transitions to that defined by the Paleozoic depositional terranes typical of the Valley and Ridge and Appalachian Plateau provinces (Fig. 1) (Rodgers, 1970), which have a much thicker sedimentary cover (Muehlberger et al., 1967). The character of the regional seismic-wave propagation is expected to be affected by passage through these contrasting terranes.

The purpose of this study is to present observations of the regional seismic wavefield generated by the Virginia earthquake

and to characterize aspects of eastern U.S. crustal structure. This is done through modeling the regional seismic-wave propagation through one-dimensional (1D; radially varying) structures appropriate for the Piedmont–Blue Ridge and Valley and Ridge–Appalachian Plateau provinces. Modeling of the regional seismograms with synthetic seismograms on a spherically symmetric Earth structure shows that the observed seismic wavefield generated by the Mineral earthquake in the eastern United States is determined primarily by wave propagation through a crustal waveguide, with the thickness of shallow sedimentary rocks playing a chief role in determining the amplitude and dispersion of the surface waves.

DATA SET

We assembled three-component seismic records from 61 stations belonging to various regional networks within 900 km of the M5.8 23 August 2011 main shock (Fig. 1). Three-component seismic records for several of these stations are presented (as red traces) in Figures 2 and 3. Record sections for the vertical component are presented in Figures 4 and 5. These alternative record sections use different gain factors to focus on different parts of the seismograms: a gain factor of $\Delta^{1/2}$ (where Δ is angular propagation distance) is used in Figure 4 to correct for expected geometrical spreading of the surface waves, and a gain factor of Δ^2 is used in Figure 5 to correct for the expected distance dependence of head waves (Aki and Richards, 1980).

In this study the seismograms are low-pass filtered at a corner period of 3 s in order to focus on the regional seismic-wave propagation. This permits the identification of regional phases, as the longer period wave propagation is not complicated by strong scattering or site effects. At the same time, the periods considered are short enough to be sensitive to strong ground motion and dynamic rupture effects such as directivity.

The observed waveforms exhibit typical regional seismic phases, e.g., Pn, P, Sn, S, Rayleigh waves, and Love waves. Beyond a critical distance of Δ ~230 km, direct P and S separate from the head waves Pn and Sn, respectively. The head waves are coherent out to ~900 km for all source-receiver azimuths. Direct P is clearly visible out to more than 500 km offset for propagation paths to the northwest quadrant (Fig. 5A), but is indiscernible at other azimuths (Fig. 5B), suggesting possible disruption of the lower crustal waveguide. Direct S, however, is observed with high amplitude at all distances and azimuths. The observed Pn and Sn moveouts, at all azimuths, are ~8.2 and 4.7 km/s, respectively, which provides estimates of the average uppermost mantle seismic velocities.

A noteworthy property of the regional seismograms is the presence of relatively high amplitude and dispersed wavetrains following direct S for source-receiver azimuths φ (measured positive clockwise from due north) ranging from due west to north-northeast ($-90° \leq \varphi < 30°$ in Fig. 4A), replotted for all three components for selected stations (e.g., BINY, WVNY, and ASCO) in Figure 3. These are highly dispersed surface waves that generally arrive with group velocity slower than 3.0 km/s. The surface waves are much less dispersed at other source-receiver azimuths ($30° \leq \varphi < 270°$ in Fig. 4B), replotted for all three components for selected stations (e.g., PANJ, CNNC, and GOGA in Fig. 2), and they generally arrive with group velocity faster than 3.0 km/s. The presence or absence of highly dispersed surface waves is diagnostic of the different crustal structures traversed by the propagating seismic waves. The observation of relatively high amplitude and dispersed surface wavetrains, when they exist, on the radial and vertical components, rather than the transverse component, suggests that the regional crustal structure affects primarily the Rayleigh waves, rather than the Love waves. This interpretation is supported by modeling of synthetic seismograms discussed in the following.

As noted by Hough (2012), the U.S. Geological Survey (USGS) community shakemap (http://earthquake.usgs.gov/earthquakes/shakemap/global/shake/082311a/) for the Mineral event (Fig. 6) indicates maximum felt intensities to the northeast of the rupture. These intensities are qualitatively comparable with maximum instrumentally recorded ground velocity. The maximum vertical-component velocities at regional broadband stations at 3 s period are shown in Figure 7. The pattern in Figure 7A is consistent with the tendency in the community shakemap for felt intensities to be largest to the northeast. The pattern corrected for geometrical spreading of the surface waves in Figure 7B, however, suggests that recorded seismic-wave energy is largest in two directions, to the north-northwest and northeast. The amplification at north-northwest azimuths is also seen in individual recordings (e.g., O56A in Fig. 3).

METHODS

In order to better understand the observations of regional seismic-wave propagation, we explore models of wave propagation through appropriate spherically symmetric models of the seismic structure. Synthetic seismograms are generated using the direct Green's function (DGF) method of Friederich and Dalkolmo (1995). This method synthesizes the seismic wavefield for a spherically layered structure of seismic velocities Vp (compressional wave) and Vs (shear wave), density ρ, and attenuation factors $Q\kappa$ and $Q\beta$ in the $l - \omega$ domain, where l denotes spherical harmonic degree and ω angular frequency. It is the spherical equivalent of the frequency-wave number method employed for flat-layered structures (e.g., Zhu and Rivera, 2002). It was coded by one of us (Pollitz, personal data) and validated against analytic solutions, including those for elastic-wave propagation in a full space for both isotropic and shear sources (equation 4.29 of Aki and Richards, 1980) and in a half-space, e.g., Lamb's problem (Kuhn, 1985), as well as the independent numerical solutions AXITRA (Bouchon, 1981) and f-k (frequency–wave number) method (Zhu and Rivera, 2002).

In order to synthesize seismic-wave propagation through laterally varying models, we use the spectral element method (SEM) (e.g., Komatitsch and Vilotte, 1998; Komatitsch and Tromp, 1999, 2002). We simulate 2.5D wave propagation (3D

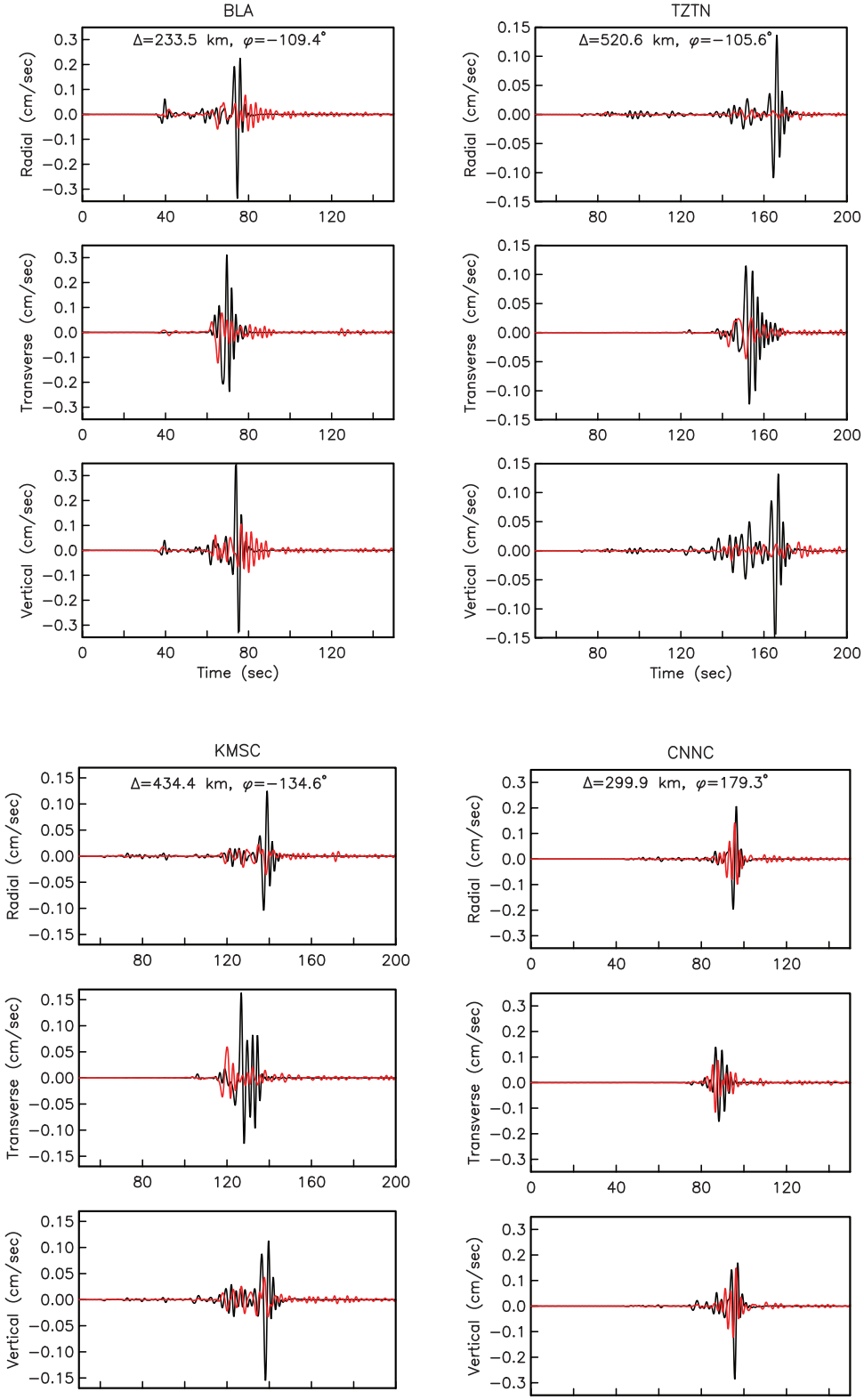

Figure 2 (*Continued on facing page*). Red lines show three-component seismograms at selected stations (locations in Fig. 1), all corresponding to paths with 30° ≤ φ < 270°, where φ is the source-receiver azimuth measured positive clockwise from due north, i.e., wave propagation through predominantly the Valley and Ridge and Appalachian Plateau provinces. Black lines show corresponding synthetic seismograms in model 1 (see Fig. 8A). Both observed and synthetic seismograms have been low-pass filtered at a corner period of 3 s. The epicentral distance and azimuth to each station are indicated.

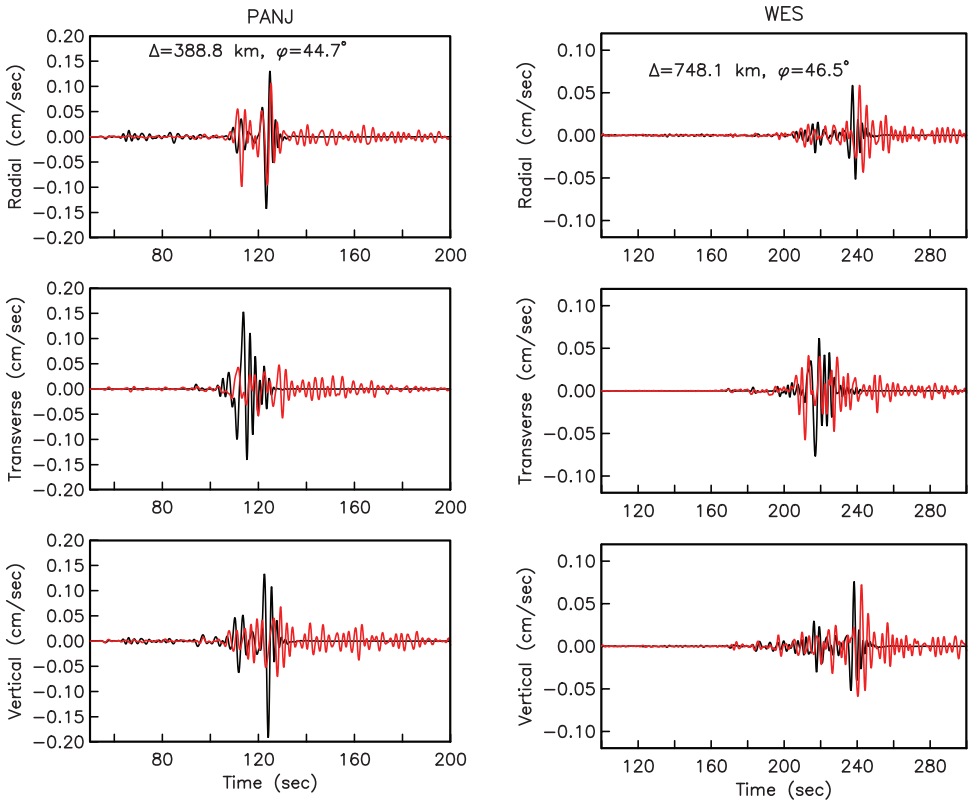

Figure 2 (*Continued*).

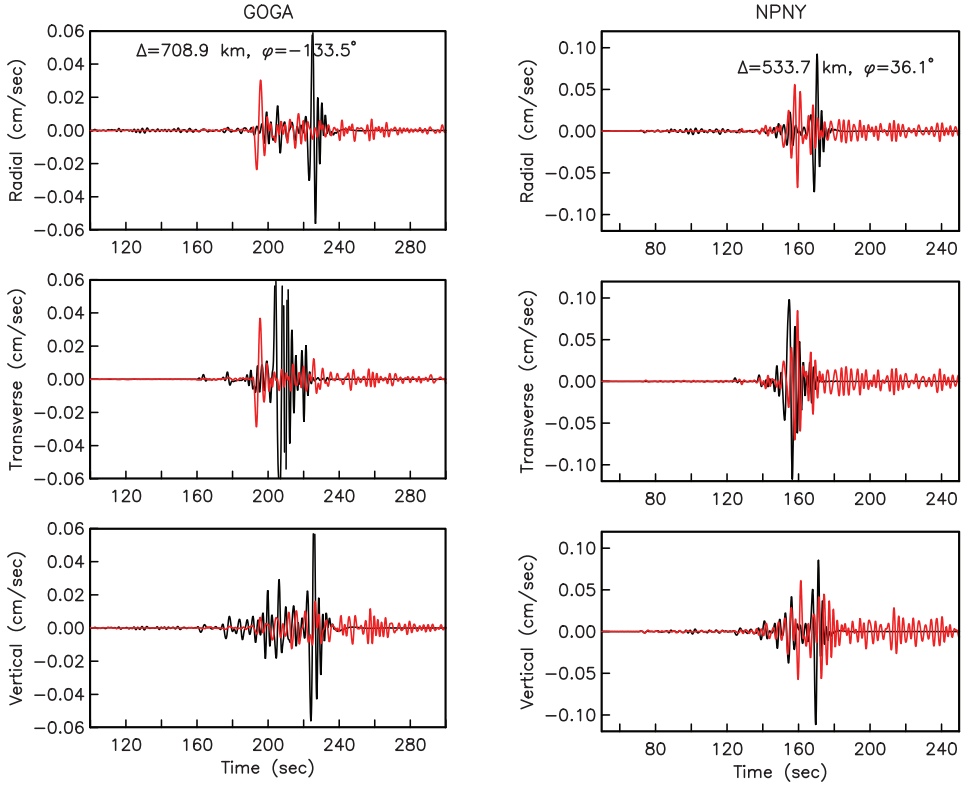

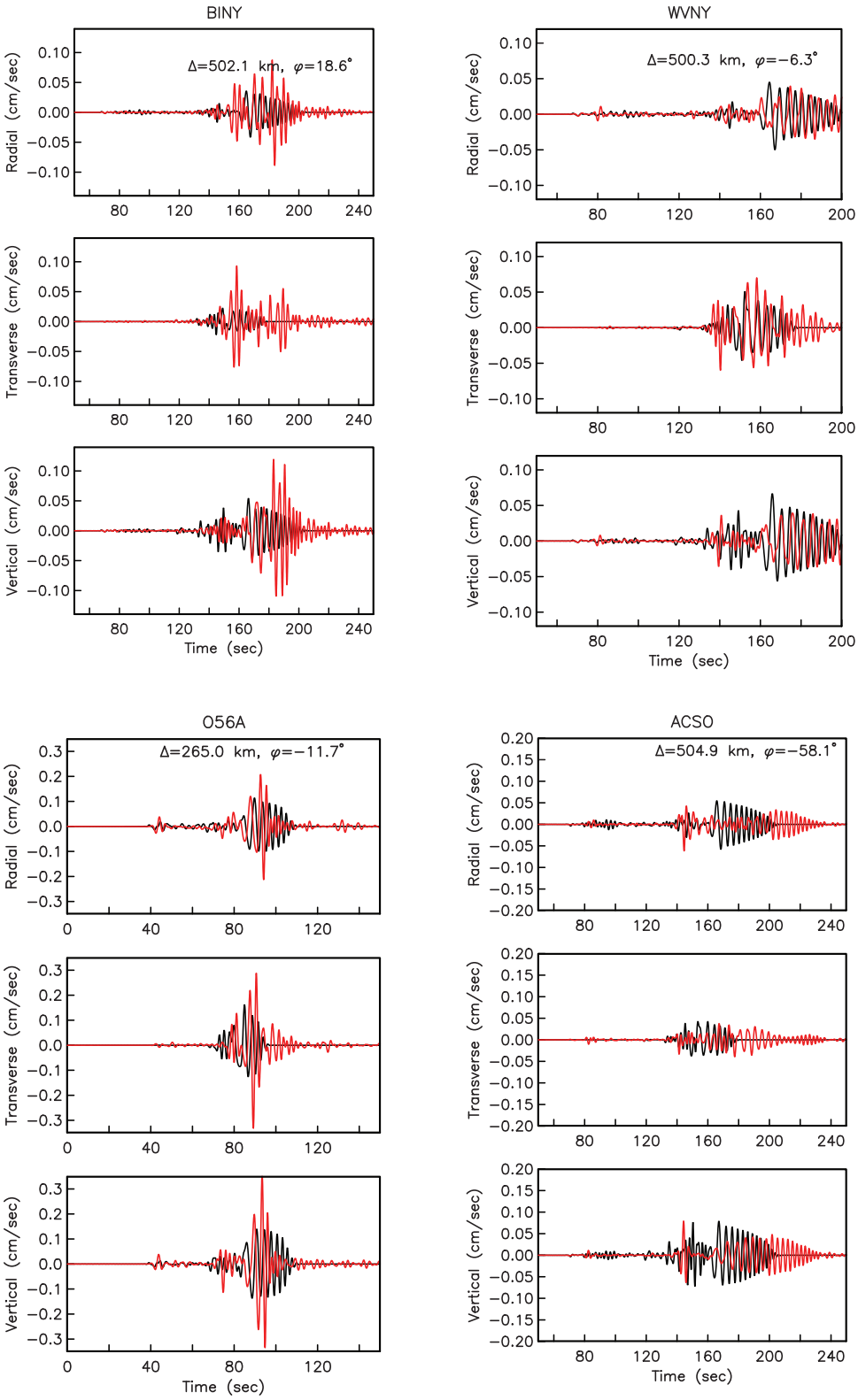

Figure 3 (*Continued on facing page*). Red lines show three-component seismograms at selected stations (locations shown in Fig. 1), all corresponding to paths with $-90° \leq \varphi < 30°$, where φ is the source-receiver azimuth measured positive clockwise from due north, i.e., wave propagation through predominantly the Piedmont, Blue Ridge, and coastal plain provinces. Black lines show corresponding synthetic seismograms in model 2 (see Fig. 8B). Both observed and synthetic seismograms have been low-pass filtered at a corner period of 3 s. The epicentral distance and azimuth to each station are indicated.

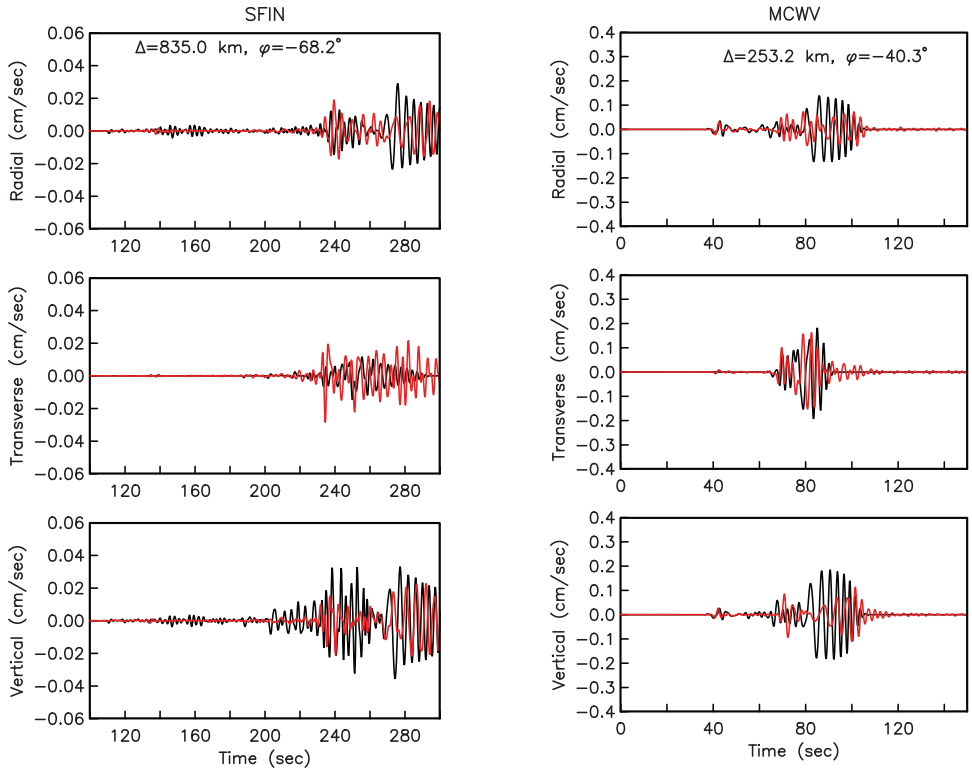

Figure 3 (*Continued*).

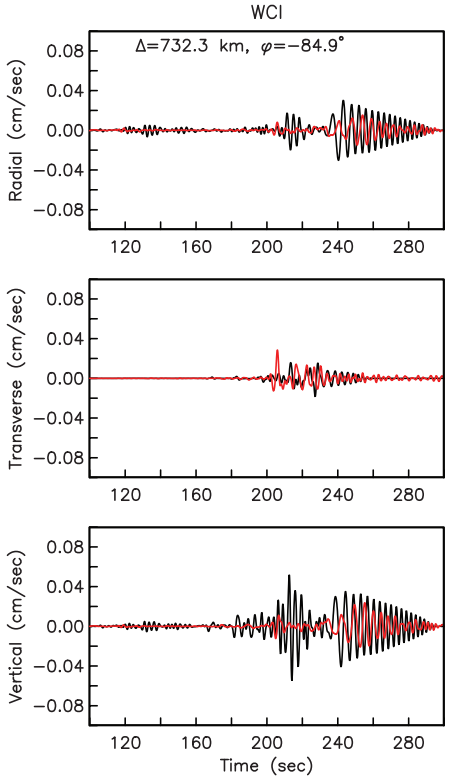

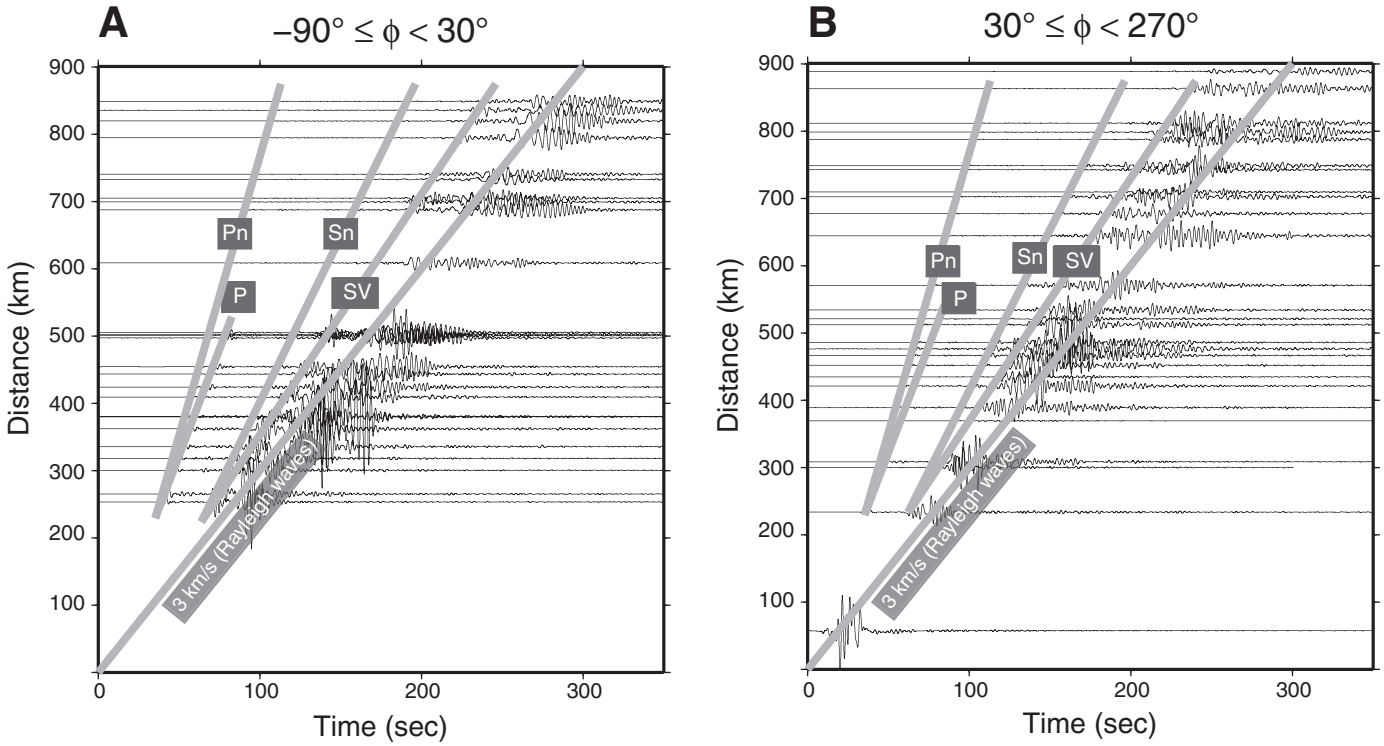

Figure 4. Record section of vertical-component seismograms, low-pass filtered at a corner period of 3 s. A gain factor proportional to $\Delta^{1/2}$ has been applied in order to correct for the geometrical spreading expected for the surface waves. Seismograms are edited according to source-receiver azimuths, where φ is the source-receiver azimuth measured positive clockwise from due north. Gray lines delineate arrival times of noted phases. Pn, Sn—longitudinal and transverse waves (head waves); P—direct longitudinal wave; SV—transverse wave with motion in a vertical plane parallel to the propagation direction. (A) $-90° \leq \varphi < 30°$. (B) $30° \leq \varphi < 270°$.

wave propagation through a 2D model) by adapting the SEM formulation of Sinclair et al. (2007) to a spherical geometry. We assume that the seismic structure is azimuthally symmetric about a prescribed Euler pole. The seismic source may be placed anywhere within the model domain; the model domain does not include the pole of symmetry, which distinguishes the application here from that of Nissen-Meyer et al. (2007). Wavefields are simulated in the frequency domain using a spatial and temporal Fourier decomposition of the seismic wavefield. A double spatial and temporal inverse Fourier transform then yields time domain results.

REGIONAL WAVE PROPAGATION

Laterally Homogeneous Sedimentary Cover Thickness

The DGF method is applied to the Virginia earthquake source in two spherically layered structures given in Figure 8 and Table 1. The first structure (model 1; Fig. 8A) is a typical eastern U.S. crustal structure and is based on Taylor (1989); it has a 1-km-thick sedimentary cover. The second structure (model 2; Fig. 8B) is modified from the first to have a 3-km-thick sedimentary cover, based on basin sedimentary rock thicknesses (Muehlberger et al., 1967). Both models have a Moho thickness of 40 km, which is consistent with other regional crustal studies (Li et al., 2003; Viegas et al., 2010). We find that these two end-member models are sufficient to replicate the main features of the observed seismic waveforms for most of the seismograms we have analyzed. The objective of exploring these models is to qualitatively match the arrival times of body-wave phases and the amplitude and duration of the surface waves. We do not attempt quantitative waveform comparisons.

We fixed the epicenter of the event based on the USGS/SLU (Saint Louis University) Regional Moment Solution (37.936°N, 77.933°W; strike 26°, dip 55°, rake 108°, seismic moment = 4.6×10^{17} N m), which is close to the epicenter and focal mechanism determinations of Chapman (2013). We variably explored source depths ranging from 5 to 12 km, which spans the range of source depths reported by various agencies. Through visual comparison of observed and synthetic seismograms we determined that a depth of 6 km yields the best agreement between these sets of waveforms.

To illustrate the regional wave propagation we calculated record sections of three-component displacement on a fictitious array of surface seismometers extending 1000 km from the epicenter. Record sections in model 1 are shown in Figures 9 and

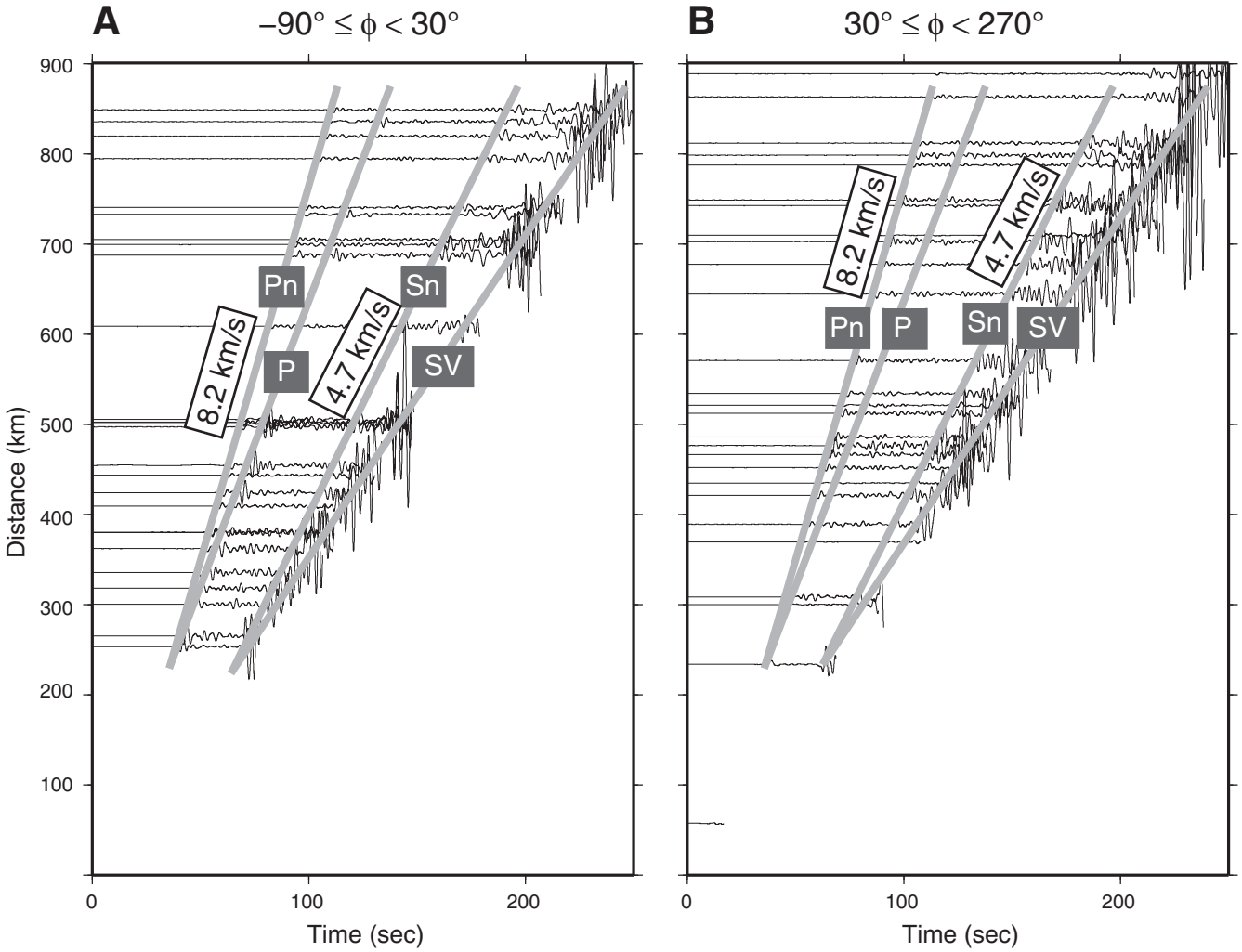

Figure 5. Record section of vertical-component seismograms, replotted from Figure 4 for propagation velocity >3.4 km/s (to remove surface-wave arrivals). A gain factor proportional to Δ^2 has been applied in order to correct for the distance dependence of amplitude expected for the head waves Pn and Sn (longitudinal and transverse waves). P—direct longitudinal wave; SV—transverse wave with motion in a vertical plane parallel to the propagation direction. Seismograms are edited according to source-receiver azimuths, where φ is the source-receiver azimuth measured positive clockwise from due north. (A) $-90° \leq \varphi < 30°$. (B) $30° \leq \varphi < 270°$.

10A using different gain factors. Corresponding record sections for model 2 are shown in Figures 11 and 10B. The main wave types generated in the synthetics are P, SV (transverse wave with motion in a vertical plane parallel to the propagation direction), and Rayleigh waves. Though SH (transverse wave with horizontal motion perpendicular to the propagation direction) and Love waves are generated at other source-receiver azimuths, the configuration used here, given the focal mechanism, generates relatively little energy on the transverse component. For both models, direct P is of highest amplitude at subcritical distance (<~230 km) but persists out to ~500 km, mimicking the observed range of direct P at least for propagation paths to the northwest quadrant (Fig. 5A). However, the head waves Pn and Sn are discernible out to 1000 km distance, mimicking the large range of observed head waves (Fig. 5). The moveout velocity of synthetic Pn and Sn are 8.18 and 4.72 km/s, respectively, in agreement with the moveout velocity of the observed phases (Fig. 5). This and the agreement of synthetic and observed arrival times of these waves (as a function of distance from the source) indicate that both the Moho depth and uppermost mantle velocity are well represented by the reference velocity structure.

In model 1 the Rayleigh and Love waves are relatively little dispersed, and there is little separation of the SH and Love wave arrivals on the transverse component. Surface waves are more highly dispersed in model 2 (Figs. 11 and 10B). Comparing Figures 9 and 11, this greater dispersion is most apparent for the Rayleigh waves, but it also disperses the Love waves enough to produce noticeable separation between SH and Love waves.

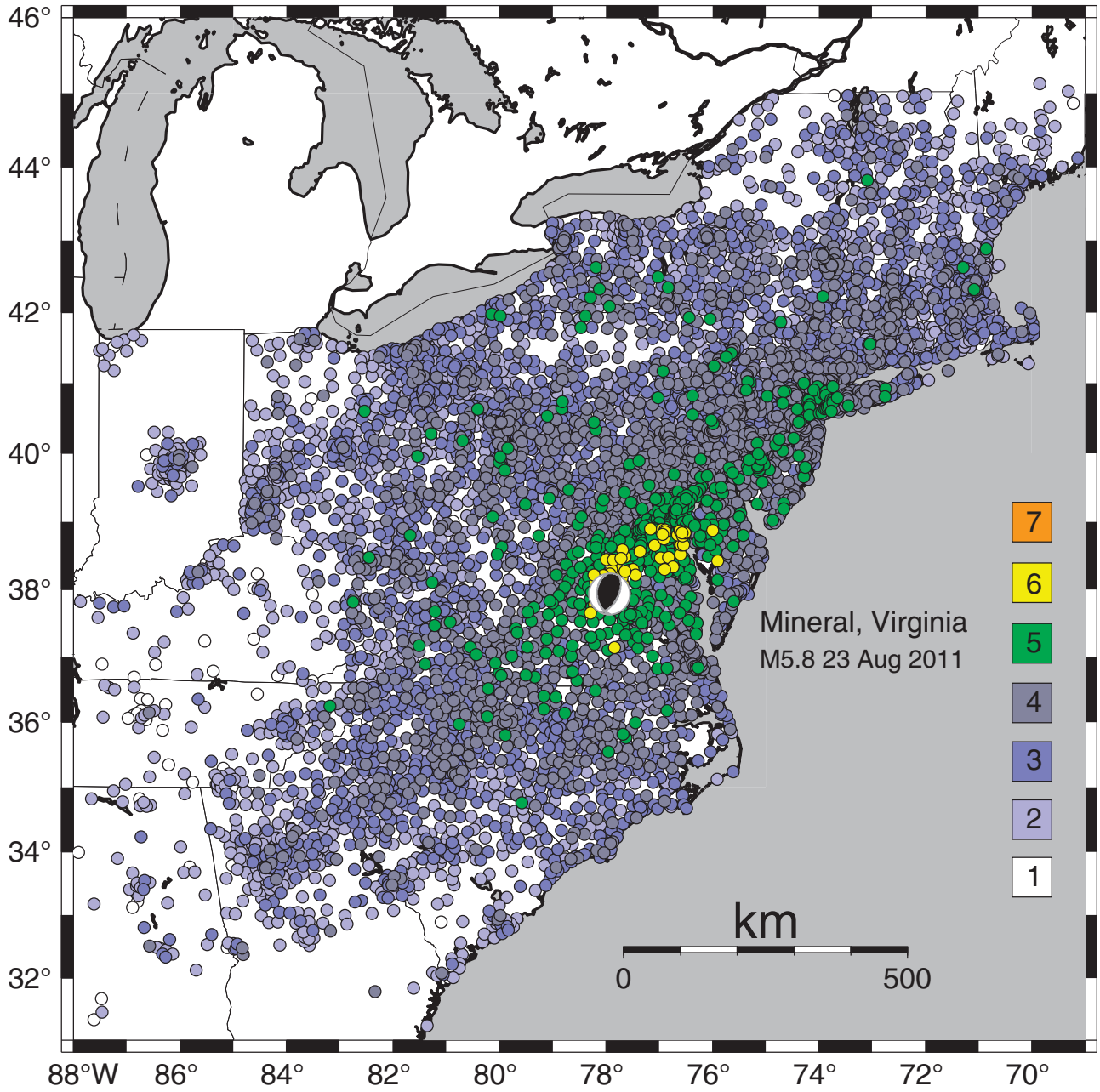

Figure 6. Community intensity map aggregated by U.S. Postal Service ZIP code for the 2011 Mineral, Virginia, earthquake from http://earthquake.usgs.gov/earthquakes/dyfi/events/se/082311a/us/index.html.

This highlights the effect of the higher sedimentary rock thickness in model 2.

Comparing observed seismograms with synthetic seismograms generated on the two velocity structures (Fig. 8), we find that observed waveforms at stations that do not exhibit the highly dispersed waves are well described to first order by synthetic seismograms in model 1 (Fig. 2), whereas observed waveforms that exhibit the relatively large amplitude wavetrains are well described by synthetic seismograms in model 2 (Fig. 3). The observed amplitudes of observed Rayleigh waves are matched by the synthetics at most, but not all, stations in Figure 2 and 3. Model 1 overestimates the observed Rayleigh wave amplitude at several stations that involve propagation paths that partially sample the Valley and Ridge Province (e.g., BLA, TZTN, GOGA); these propagation paths are better described as intermediate between model 1 and model 2. The very different durations of the surface wavetrains are generally well captured by the two elastic-structure models.

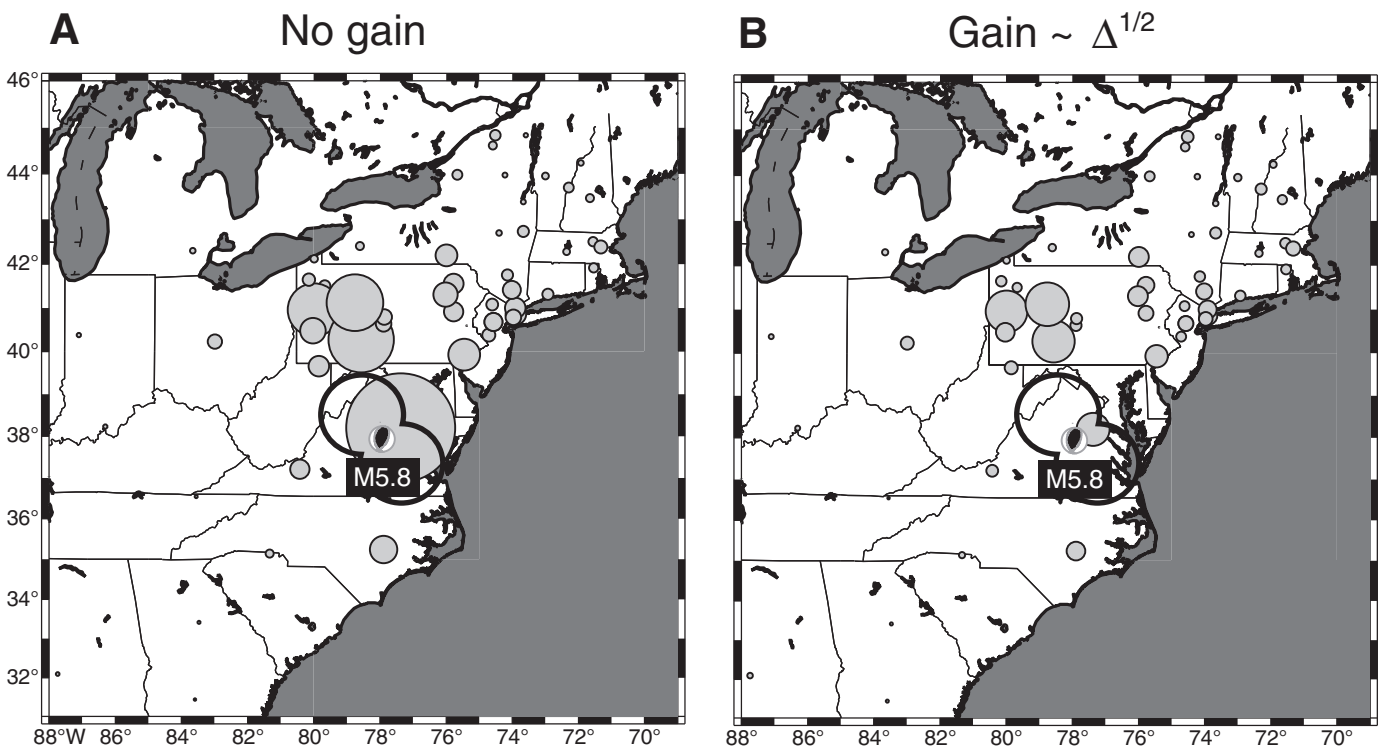

Figure 7. Maximum vertical-component velocity recorded on regional broadband seismograms filtered at 3 s period. (A) No gain factor is applied, and symbol size plotted at a seismic station is proportional to velocity. The largest circle corresponds to a velocity of 0.6 cm/s. (B) A gain factor of $\Delta^{1/2}$ is applied in order to correct for geometrical spreading expected for seismic surface waves. The earthquake focal mechanism and radiation pattern for a 3 s period fundamental-mode Rayleigh wave in model 1 are superimposed.

Laterally Heterogeneous Sedimentary Cover Thickness

We investigate 3D synthetic wave propagation through a simple 2D model of seismic structure. The eastern United States is idealized as consisting of model 2 structure within a band of width 3.12 geocentric degrees (347 km), indicated in gray in Figure 12, flanked by model 1 structure (with original Moho depth of 40 km) to its west and model 1 structure with modified Moho depth of 34 km to its east. The model 2 band is meant to represent the greater thickness of sedimentary cover in the Valley and Ridge and Appalachian Plateau regions approximately with a 2D structure. The reduced crustal thickness east of this band is consistent with crustal structure determinations (e.g., fig. 4 of Mooney and Kaban, 2010).

The symmetry axis of the structure depicted in Figure 12 is a Euler pole at 55°N, 132°W, and the model 2 domain is bounded by small circles centered on this pole (~36° away). The earthquake is implemented as a point source using the USGS/SLU solution used for the synthetics presented herein.

Figure 12 shows snapshots of the east component seismic velocity at selected times. It reveals that the seismic wavefield is profoundly modified as it enters the model 2 region on northward to westward paths from the source, leading to higher dispersion in the Rayleigh wavetrain at a dominant period of 3 s. The waves that propagate to the northeast and southwest, i.e., that remain in the model 1 domain, do not undergo such alteration in the dispersion. This is seen alternatively in snapshots of horizontal velocity in a depth slice along a northwest-southeast profile (Fig. 13), where the Rayleigh wave becomes highly dispersed as it enters the model 2 region.

The 2.5D synthetics are similar to the DGF synthetics for paths that traverse predominately areas prescribed by model 1 structure, e.g., BLA, PANJ, or KMSC in Figure 14, which are close to the corresponding DFG synthetics in Figure 2. Differences arise from the different Moho depths east of the Valley and Ridge Province assigned in the two models: 34 km in the 2.5D synthetics versus 40 km in the DGF synthetics. For other paths, the 2.5D synthetics yield a hybrid character to those synthetics generated in models 1 and 2. Surface wavetrains for such paths are slightly less dispersed and of higher amplitude than the DGF synthetics in model 2 (Fig. 3). For O56A, WVNY, and TZTN, this hybrid character of the 2.5D synthetics produces a good qualitative agreement with observed seismograms (Fig. 14). The TZTN synthetics have the same highly dispersive character as, but much greater amplitude than, the observed seismograms, suggesting strong defocusing not accounted for by the employed

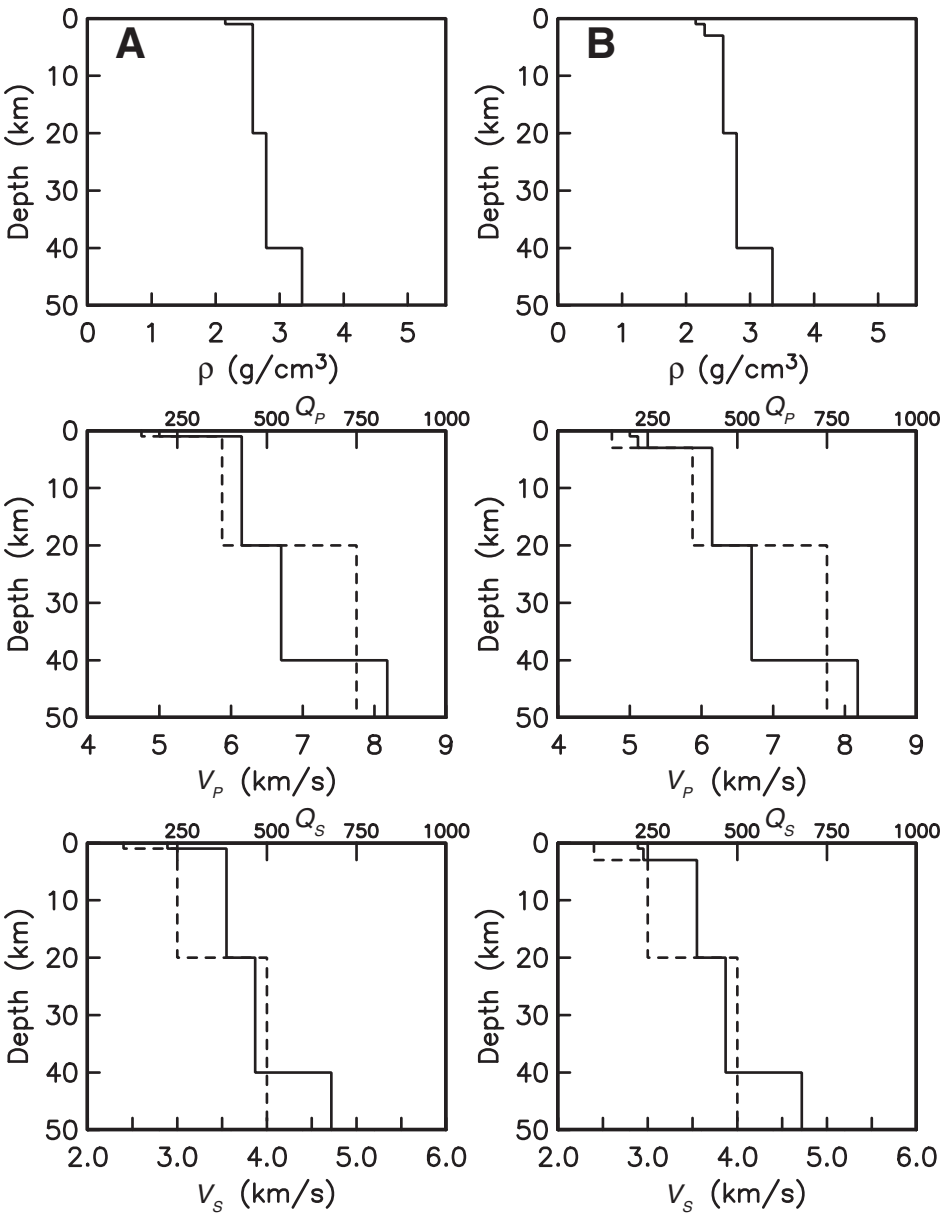

Figure 8. Layered structure of *P* and *S* velocities V_P and V_S, density ρ, and *P*- and *S*-wave attenuation factors Q_P and Q_S (dashed lines) as a function of depth. (A) Model 1. Thin sedimentary cover model, based on Taylor (1989). (B) Model 2. Thick sedimentary cover model, modified from A to have a 3-km-thick sediment layer.

TABLE 1. REFERENCE EASTERN U.S. ELASTIC STRUCTURE

Depth (km)	ρ (kg/m³)	Vp (km/s)	Vs (km/s)	Qβ*	Qκ*
0–1	2150	5.00	2.89	100	250
1–3	2580†	6.15†	3.55†	250	625
1–3	2290§	5.11§	2.95§	100	250
3–5	2580	6.15	3.55	250	625
5–20	2580	6.15	3.55	250	625
20–40	2790	6.70	3.87	500	1250
40+	3350	8.18	4.72	500	1250

Note: Structure is density common to model 1 and model 2 (see text Fig. 6) except where indicated. Vp—compressional wave velocity; Vs—shear wave velocity; ρ—density.
*Qβ, Qκ are attenuation factors.
†Model 1.
§Model 2.

structure. The 2D structure model could be improved through further consideration of variable crustal velocities (e.g., Liang and Langston, 2009), crustal thickness, surface topography, and sedimentary cover thickness.

DISCUSSION

In the context of 1D models, the difference between model 1 and model 2 is simply the thickness of the sedimentary cover, which is 1 km in model 1 and 3 km in model 2. Given the source depth of 6 km, Rayleigh waves of ~3 s period are expected to be well excited on either model, but they are highly dispersed in model 2. We propose a grouping of stations as having affinity with model 1 or model 2 based on the modeling with these

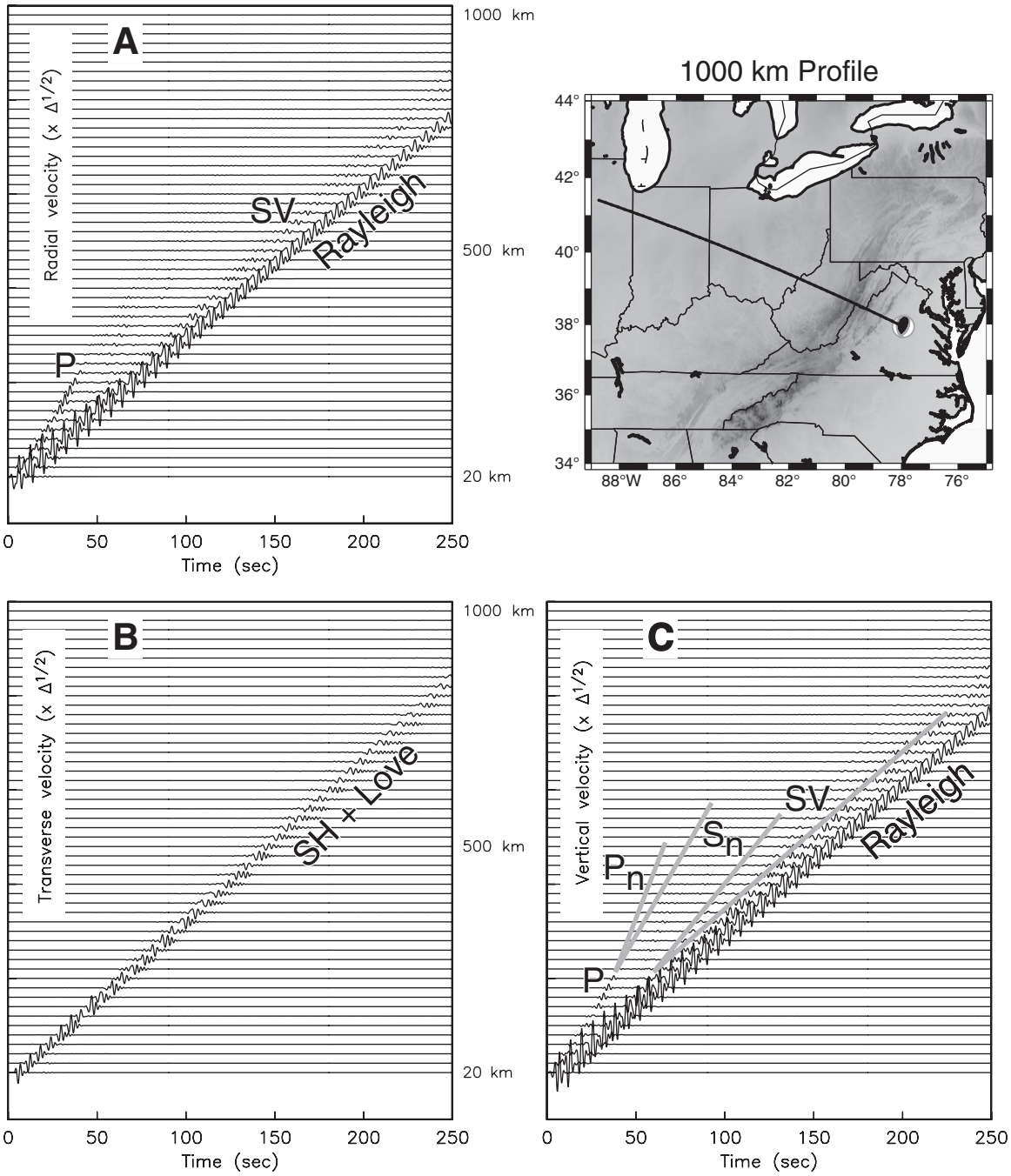

Figure 9. Synthetic record sections of velocity calculated in model 1 along a fictitious array of surface stations extending 1000 km from the Virginia earthquake epicenter (inset). (A) Radial component. P—compressional wave. SV—transverse wave with motion in a vertical plane parallel to the propagation direction. (B) Transverse component. SH—transverse wave with horizontal motion perpendicular to the propagation direction. (C) Vertical component. Gray lines delineate arrival times of noted phases. Other abbreviations as in Figure 5.

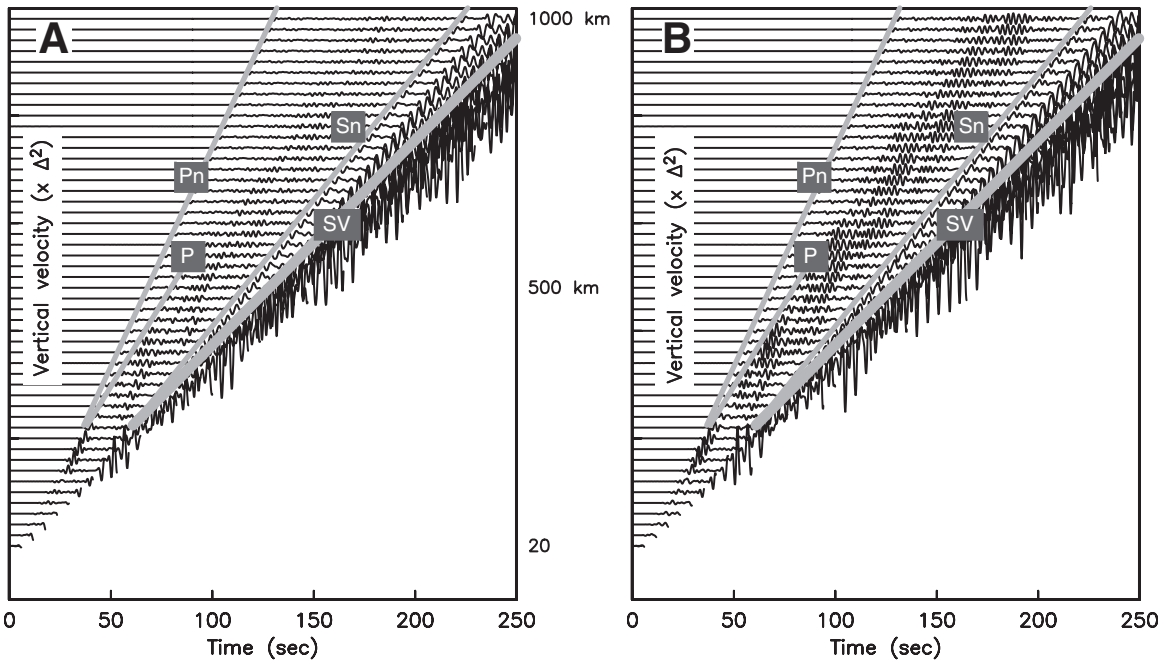

Figure 10. Synthetic record sections of vertical-component velocity replotted from Figures 9 and 11 for propagation velocity >3.4 km/s (to remove surface-wave arrivals). A gain factor proportional to Δ^2 has been applied in order to correct for the distance dependence of amplitude expected for the head waves Pn and Sn. (A) Model 1. (B) Model 2. Gray lines delineate arrival times of noted phases. Abbreviations as in Figure 5.

laterally homogeneous structures. This grouping is illustrated in Figure 15 and follows the grouping of record sections of observed seismograms in Figure 4.

The Piedmont and Blue Ridge provinces constitute the "crystalline Appalachians"; together with the central and northern Appalachians they have modest (<~1 km) sedimentary cover. The Valley and Ridge Province and Appalachian Plateau constitute the "sedimentary Appalachians," which have a sedimentary cover thickness of 1.5–7.5 km (Muehlberger et al., 1967). Large sedimentary cover thickness persists to the north and northwest of the Appalachian Plateau (fig. 4 of Mooney and Kaban, 2010), e.g., the Illinois Basin. The stations in the two groups identified in Figure 15 are spatially clustered: one group exhibits strongly dispersive Rayleigh waves having crustal propagation paths that pass through the sedimentary Appalachians; the other group corresponds to propagation paths that pass through the crystalline Appalachians or the coastal plain.

At a 3 s period, the effect of sedimentary cover thickness on the length of the Rayleigh surface wavetrain is found to be considerable for a thickness of ~3 km, about one-third the wavelength of the Rayleigh wave. A similar dependence of surface-wave duration on the thickness of a low-velocity surface layer is seen in the basin response to incident Rayleigh waves (e.g., Kawase and Aki, 1989). The fact that Love waves are less sensitive to sediment thickness, both observationally (the transverse-component seismograms in Figs. 2 and 3) and in the synthetics (the transverse-component seismograms in Figs. 2, 3, 9, and 11), is attributable to the greater wavelength of Love waves and correspondingly smaller ratio of sediment thickness to wavelength.

The proposed grouping, while providing an explanation for observed surface-wave duration, may only partially explain the tendency for observed maximum ground velocity to be largest along north-northwest and northeast azimuths from the source epicenter (Fig. 7). The 2.5D simulations of the seismic wavefield presented in Figure 12 indicate that these areas of large amplitude are anomalous, i.e., not explicable with purely 2D structural variations or expected variations in the surface-wave radiation pattern with azimuth. For paths to the north-northwest, comparison of calculated record sections (Figs. 9 and 11) indicate that a modest increase in sediment thickness to 3 km from a reference value of 1 km tends to increase dispersion while reducing group amplitudes, and so does not produce the anomalously large amplitudes to the north-northwest. We suggest that the high-amplitude lobe toward western Pennsylvania may arise from locally large sediment thickness (locally exceeding 8 km) in the northern Valley and Ridge Province (Frezon et al., 1983). This would amplify Rayleigh wave group arrivals through lateral focusing. The northeast lobe may arise from source directivity. This is supported by the strong asymmetry in maximum velocity between areas to the northeast and southwest of the epicenter (Fig. 7B). It is also suggested by the modeling of felt intensities in figure 4 of Hough (2012). Chapman (2013, figs. 16 and 17 therein) inferred

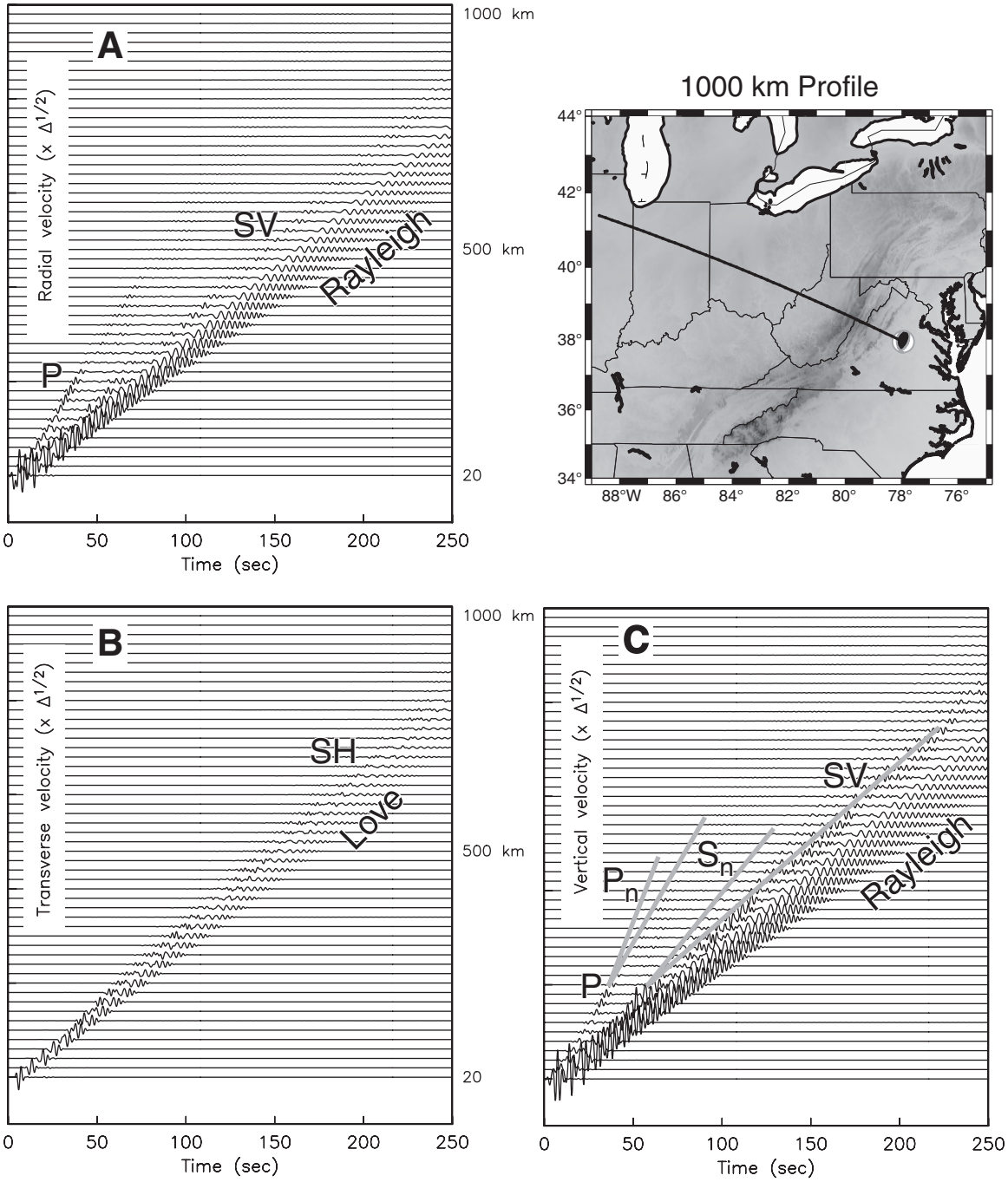

Figure 11. Synthetic record sections of velocity calculated in model 2 along a fictitious array of surface stations extending 1000 km from the Virginia earthquake epicenter (inset). (A) Radial component. (B) Transverse component. (C) Vertical component. Gray lines delineate arrival times of noted phases. Other abbreviations as in Figure 5.

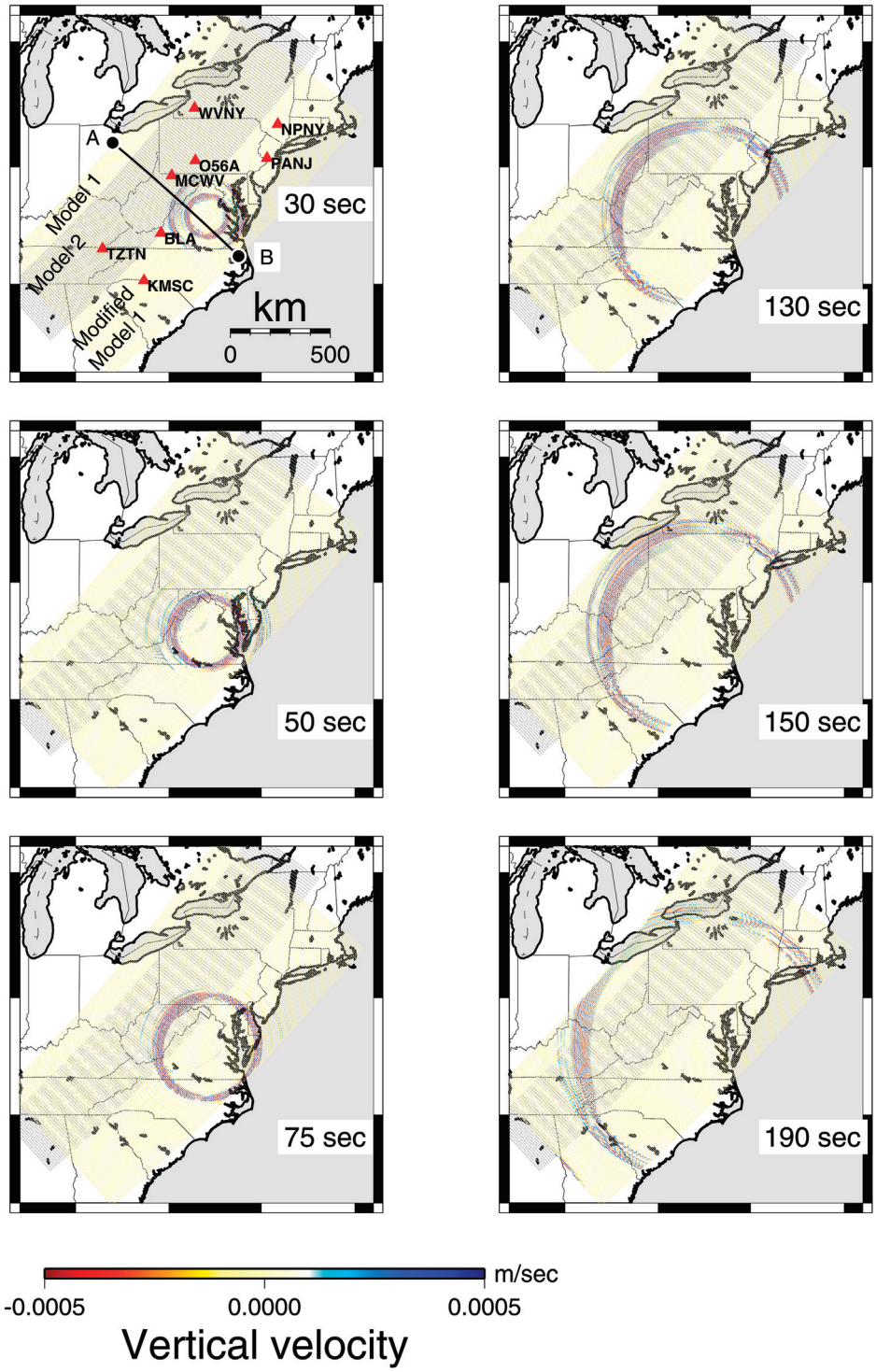

Figure 12. Snapshots of the east component seismic velocity at Earth's surface generated by 2.5 dimensional synthetics. Upper left shows A–B depth section; red triangles are seismic stations. Seismic structure is prescribed by model 2 (see Fig. 8) in the gray region, with adjacent regions to the west and east assigned as, respectively, model 1 structure with original Moho depth of 40 km and model 1 structure with modified Moho depth of 34 km. Both observed and synthetic seismograms have been low-pass filtered at a corner period of 3 s.

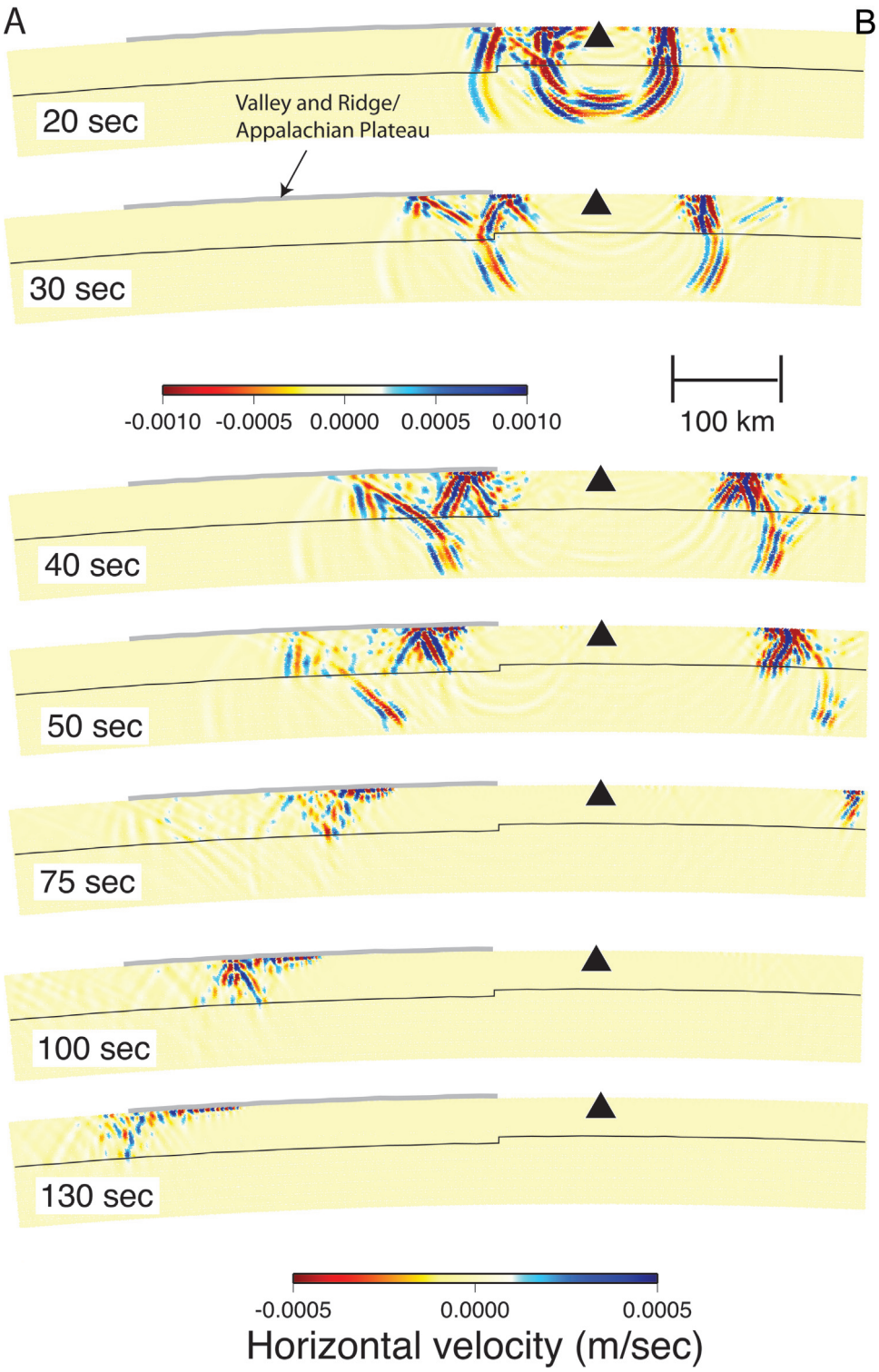

Figure 13. Snapshots of the east-component seismic velocity generated by 2.5 dimensional synthetics along the depth section A-B (shown in the upper left of Fig. 12). Thin black line in each snapshot indicates the Moho discontinuity. Triangles are the projection of the 2011 hypocenter along the profile.

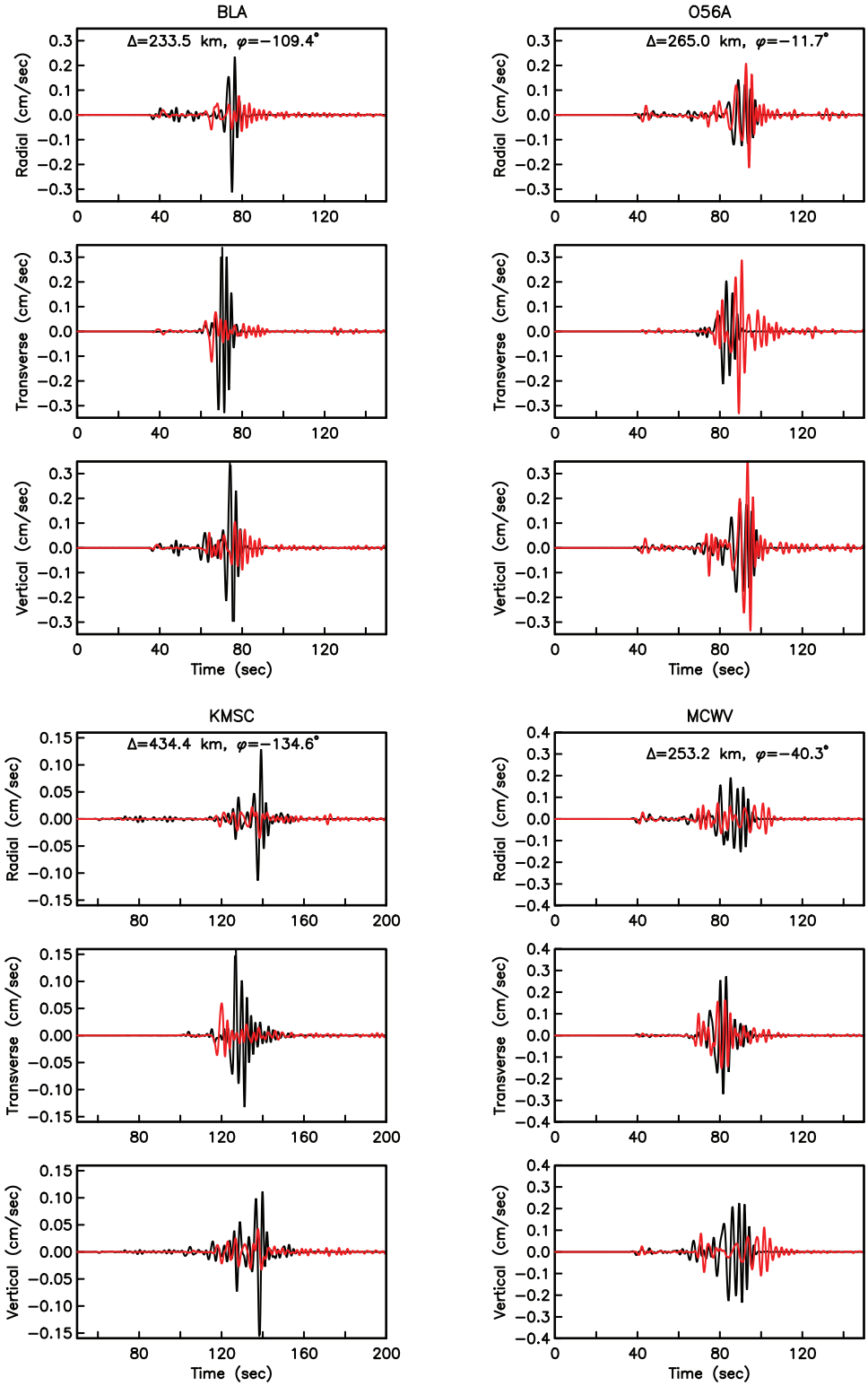

Figure 14 (*Continued on facing page*). Red lines show three-component seismograms at selected stations (locations shown in Fig. 12). Black lines show 2.5D synthetics. Epicentral distance and azimuth to each station are indicated.

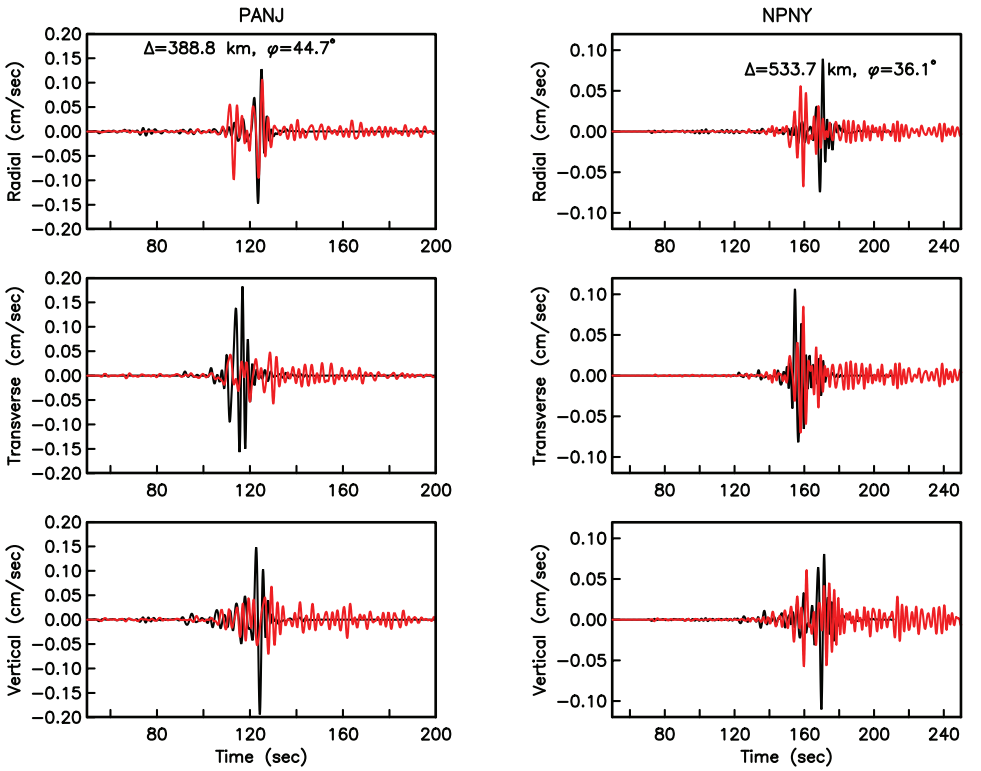

Figure 14 (*Continued*).

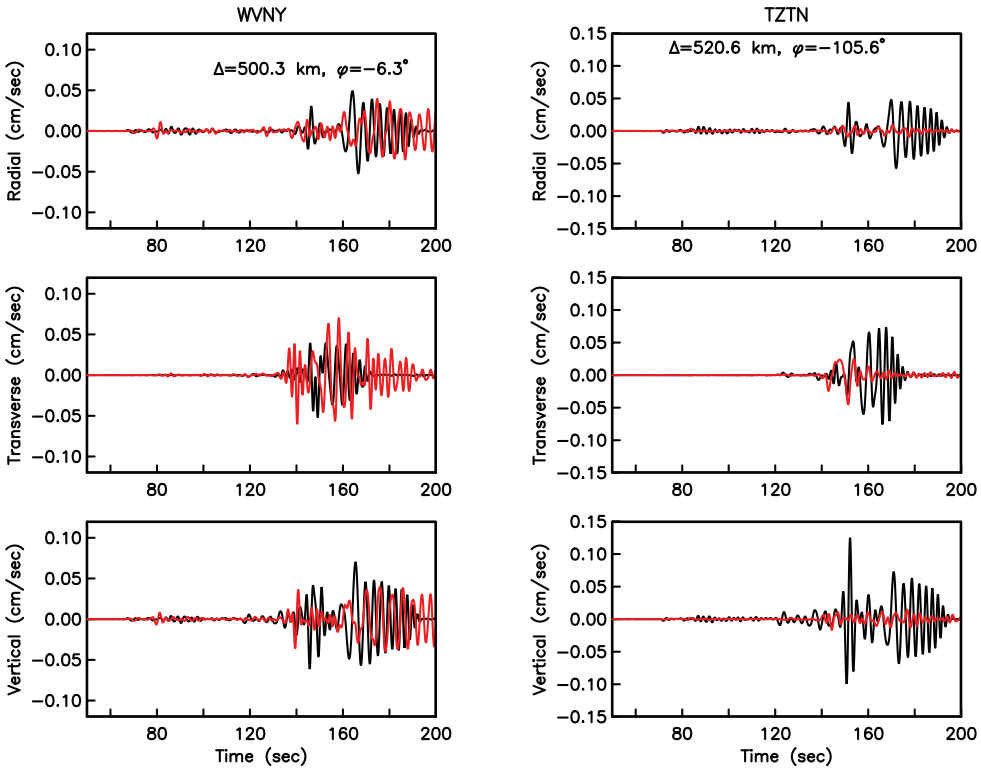

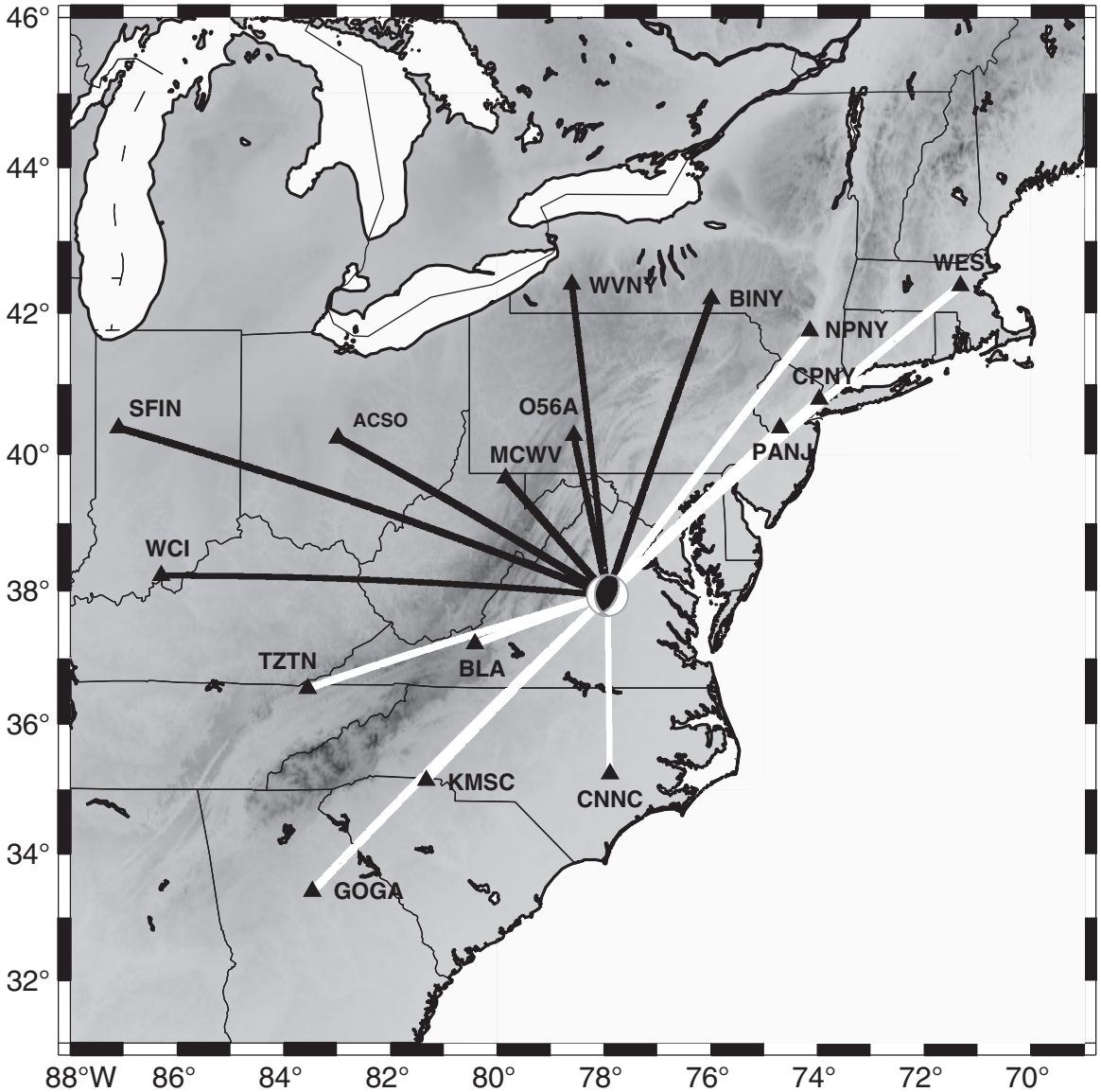

Figure 15. Summary of paths to selected stations that either exhibit strongly dispersive Rayleigh waves (black minor arcs) or weakly dispersive Rayleigh waves (white minor arcs).

northward rupture propagation based on waveform modeling, consistent with the observed asymmetry. A possible additional factor is anisotropic wave propagation arising from the regional northeast-trending tectonic fabric (Hough, 2012).

CONCLUSIONS

Seismic waves traversing the eastern United States following the M5.8 2011 Mineral, Virginia, earthquake were shaped by path effects through a laterally variable crustal structure. The path effects primarily depend on whether the propagation path passes through the Valley and Ridge and Appalachian Plateau provinces or is restricted to the Piedmont, Blue Ridge, and Coastal Plain provinces. The exceptionally thick sequences of metasedimentary rocks in the Valley and Ridge and the Appalachian Plateau affect the Rayleigh waves by profoundly increasing their dispersion, resulting in a lengthening of the arriving surface wavetrains.

Regional body-wave propagation is dominated by direct P and S, which are confined to a lower crustal waveguide and are consistent with a reference eastern U.S. structure that has constant crustal thickness of 40 km. Systematic differences exist in the sharpness of the direct P arrival with distance, with observed direct P amplitudes in the $-90° \leq \varphi < 30°$ source-receiver azimuth range being larger than those observed at other azimuths.

This suggests corresponding lateral variations in the continuity of the lower crust (e.g., less scattering at northwest to north azimuths) and/or systematic variations in crustal thickness (e.g., Braile et al., 1989; Mooney and Kaban, 2010; Abt et al., 2010).

Peak ground velocity is relatively large to northeast azimuths from felt intensities at ~1 Hz, as well as northern azimuths from broadband recordings at longer period. This pattern is not explicable with the source radiation pattern, which predicts maximum Rayleigh wave amplitudes to the northwest, or 2D lateral variation parallel to the Appalachian Mountains. The observations imply that directivity effects combined with focusing and/or defocusing effects from regional 3D structure are important in determining the peak ground motions. The origins of the anomalously high radiated seismic-wave energy are important for understanding the variability in ground motions expected for an earthquake in the eastern United States (e.g., Somerville et al., 2001; Hines et al., 2010), and they merit further study.

ACKNOWLEDGMENTS

We are grateful to the Incorporated Research Institutions for Seismology (IRIS) for archiving and making available the broadband data used in this study. Data were provided by the IRIS Data Management Center. We used data from the following regional networks: US, LD (Lamont-Doherty Cooperative Seismographic Network), TA (Earthscope Transportable Array), PE (Penn State Network), IU (IRIS/USGS Global Seismograph Network), NE (New England Seismic Network), and IM (International-Miscellaneous Stations). We acknowledge the support of the U.S. Geological Survey National Earthquake Hazards Program, and the encouragement of R.A. Williams, T. Brocher, W. Leith, and M. Blanpied. Discussions with M. Chapman and reviews by Arthur Snoke and an anonymous reviewer are gratefully acknowledged.

REFERENCES CITED

Abt, D.L., Fischer, K.M., French, S.W., Ford, H.A., Yuan, H., and Romanowicz, B., 2010, North American lithospheric discontinuity structure imaged by Ps and Sp receiver functions: Journal of Geophysical Research, v. 115, doi:10.1029/2009JB006914.

Aki, K., and Richards, P.G., 1980, Quantitative Seismology, Volume 1: San Francisco, W.H. Freeman and Company, 557 p.

Bailey, C.M., and Owens, B.E., 2012, Traversing suspect terranes in the central Virginia Piedmont: From Proterozoic anorthosites to modern earthquakes, *in* Eppes, M.C., and Bartholomew, M.J., eds., From the Blue Ridge to the Coastal Plain: Field Excursions in the Southeastern United States: Geological Society of America Field Guide 29, p. 327–344, doi:10.1130/2012.0029(10).

Bouchon, M., 1981, A simple method to calculate Green's functions for elastic layered media: Seismological Society of America Bulletin, v. 71, p. 959–971.

Braile, L., Hinze, W., von Frese, R., and Keller, G., 1989, Seismic properties of the crust and uppermost mantle of the conterminous United States and adjacent Canada, *in* Pakiser, L., and Mooney, W., eds., Geophysical Framework of the Continental United States: Geological Society of America Memoir 172, p. 655–680, doi:10.1130/MEM172-p655.

Chapman, M.C., 2013, On the rupture process of the 23 August 2011 Virginia earthquake: Seismological Society of America Bulletin, v. 103, p. 613–628, doi:10.1785/0120120229.

Cloetingh, S., Beekman, F., Ziegler, P., van Wees, J., and Sokoutis, D., 2008, Post-rift compressional reactivation potential of passive margins and extensional basins, *in* Johnson, H., Doré, T.G., Gatliff, R.W., Holdsworth, R.W., Lundin, E., and Ritchie, J.D., eds., Nature and Origin of Compression in Passive Margins: Geological Society, London, Special Publication 306, p. 27–70, doi:10.1144/SP306.2.

Coler, D., Wortman, G., Samson, S., Hibbard, J., and Stern, R., 2000, U-Pb geochronology, Nd isotopic, and geochemical evidence for the correlation of the Chopawamsic and Milton terranes, Piedmont zone, southern Appalachian orogen: Journal of Geology, v. 108, p. 363–380, doi:10.1086/314411.

Ellsworth, W.L., Imanishi, K., Luetgert, J.H., Kruger, J., and Hamilton, J., 2011, The Mw 5.8 Virginia earthquake of August 23, 2011 and its aftershocks: A shallow high stress drop event: American Geophysical Union, Fall Meeting 2011, abs. S14B-05.

Farrar, S., and Owens, B., 2001, A north-south transect of the Goochland terrane and associated A-type granites Virginia and North Carolina, *in* Hoffman, C.W., ed., Field Trip Guidebook: 50th Annual Meeting of the Southeastern Section, Geological Society of America, Raleigh, North Carolina, p. 75–92.

Farrar, S.S., 1984, The Goochland granulite terrane; remobilized Grenville basement in the eastern Virginia Piedmont, *in* Bartholomew, M.J., ed., The Grenville Event in the Appalachians and Related Topics: Geological Society of America Special Paper 194, p. 215–227, doi:10.1130/SPE194-p215.

Frezon, S.I., Finn, T.M., and Lister, J.H., 1983, Total thickness of sedimentary rocks in the conterminous United States: U.S. Geological Survey Open-File Report 83-920, 1 map, 63 × 98 cm, scale ~1:5,000,000.

Friederich, W., and Dalkolmo, J., 1995, Complete synthetic seismograms for a spherically symmetric Earth by a numerical computation of the Green's function in the frequency domain: Geophysical Journal International, v. 122, p. 537–550, doi:10.1111/j.1365-246X.1995.tb07012.x.

Glover, L.I., Mose, D., Costain, J., Poland, F., and Reilly, J., 1982, Grenville basement in the eastern Piedmont of Virginia; a progress report: Geological Society of America Abstracts with Programs, v. 14, no. 1–2, p. 20.

Hines, E.M., Baise, L.G., and Swift, S.S., 2010, Ground-motion suite selection for eastern North America: Journal of Structural Engineering, v. 137, p. 358–366, doi:10.1061/(ASCE)ST.1943-541X.0000258.

Hough, S.E., 2012, Initial assessment of the intensity distribution of the 2011 Mw 5.8 Mineral, Virginia earthquake: Seismological Research Letters, v. 83, p. 649–657, doi:10.1785/0220110140.

Kawase, H., and Aki, K., 1989, A study on the response of a soft basin for incident S, P, and Rayleigh waves with special reference to the long duration observed in Mexico City: Seismological Society of America Bulletin, v. 79, p. 1361–1382.

Komatitsch, D., and Tromp, J., 1999, Introduction to the spectral element method for three-dimensional seismic wave propagation: Geophysical Journal International, v. 139, p. 806–822, doi:10.1046/j.1365-246x.1999.00967.x.

Komatitsch, D., and Tromp, J., 2002, Spectral element simulations of global seismic wave propagation—I: Validation: Geophysical Journal International, v. 149, p. 390–412, doi:10.1046/j.1365-246X.2002.01653.x.

Komatitsch, D., and Vilotte, J., 1998, The spectral-element method: An efficient tool to simulate the seismic response of 2D and 3D geological structures: Seismological Society of America Bulletin, v. 88, p. 368–392.

Kuhn, M.J., 1985, A numerical study of Lamb's Problem: Geophysical Prospecting, v. 33, p. 1103–1137, doi:10.1111/j.1365-2478.1985.tb01355.x.

Li, A., Forsyth, D.W., and Fischer, K.M., 2003, Shear velocity structure and azimuthal anisotropy beneath eastern North America from Rayleigh wave inversion: Journal of Geophysical Research, v. 108, 2362, doi:10.1029/2002JB002259.

Liang, C., and Langston, C.A., 2009, Three-dimensional crustal structure of eastern North America extracted from ambient noise: Journal of Geophysical Research, v. 114, doi:10.1029/2008JB005919.

Mooney, W.D., and Kaban, M.K., 2010, The North American upper mantle: Density, composition, and evolution: Journal of Geophysical Research, v. 115, B12424, doi:10.1029/2010JB000866.

Muehlberger, W.R., Denison, R.E., and Lidiak, E.G., 1967, Basement rocks in continental interior of United States: American Association of Petroleum Geologists Bulletin, v. 51, p. 2351–2380.

Neuschel, S., 1970, Correlation of aeromagnetics and aeroradioactivity with lithology in the Spotsylvania area, Virginia: Geological

Society of America Bulletin, v. 81, p. 3575–3589, doi:10.1130/0016-7606(1970)81[3575:COAAAW]2.0.CO;2.

Nissen-Meyer, T., Fournier, A., and Dahlen, F.A., 2007, A two-dimensional spectral-element method for computing spherical-earth seismograms—I. Moment-tensor source: Journal of Geophysical Research, v. 168, p. 1067–1092, doi:10.1111/j.1365-246X.2006.03121.x.

Pavlides, L., 1981, The central Virginia volcanic-plutonic belt; an island arc of Cambrian(?) age: U.S. Geological Survey Professional Paper 1231-A, 34 p.

Rodgers, J., 1970, The Tectonics of the Appalachians: New York, Wiley-Interscience, 271 p.

Sinclair, C., Greenhalgh, S., and Zhou, B., 2007, 2.5D modeling of elastic waves in transversely isotropic media using the spectral element method: Exploration Geophysics, v. 38, p. 225–234, doi:10.1071/EG07025.

Somerville, P., Collins, N., Abrahamson, N., Graves, R., and Saikia, C., 2001, Ground motion attenuation relations for the central and eastern United States: Final Report, June 30, 2001: U.S. Geological Survey contract 99HQGR0098, 38 p.

Taylor, S., 1989, Geophysical framework of the Appalachians and adjacent Grenville province, *in* Pakiser, L.C., and Mooney, W.D., eds., Geophysical Framework of the Continental United States: Geological Society of America Memoir 172, p. 317–348, doi:10.1130/MEM172-p317.

Viegas, G.M., Baise, L.G., and Abercrombie, R.E., 2010, Regional wave propagation in New England and New York: Seismological Society of America Bulletin, v. 100, p. 2196, doi:10.1785/0120090223.

Zhu, L., and Rivera, L.A., 2002, A note on the dynamic and static displacements from a point source in multilayered media: Geophysical Journal International, v. 148, p. 619–627, doi:10.1046/j.1365-246X.2002.01610.x.

Manuscript Accepted by the Society 6 June 2014
Manuscript Published Online xx Month 2014

Printed in the USA